Vacancy-solute clustering in Fe-Cr alloys after neutron irradiation

M.J. Konstantinović[a,*], A. Ulbricht[b], T. Brodziansky[d], N. Castin[a], L. Malerba[d]

[a] *Studiecentrum voor Kernenergie/Centre d'Etude de l'Energie Nucléaire (SCK•CEN), Boeretang 200, B-2400 Mol, Belgium*
[b] *Helmholtz-Zentrum Dresden-Rossendorf (HZDR), Bautzner Landstraße 400, 01328 Dresden, Germany*
[c] *Faculty of electrical engineering and information technology, Slovak University of Technology in Bratislava, Vazovova 5, 811 07 Bratislava, Slovakia*
[d] *Division of Energy Materials, CIEMAT, Avenida Complutense 40, 28040 Madrid, Spain*

Abstract

Vacancy-solute clustering in neutron irradiated Fe-Cr alloys with various concentrations of Cr and minor solutes (Ni, Si and P) were studied by using coincidence Doppler broadening spectroscopy and small angle neutron scattering techniques. The results from both experiments, supported by the object kinetic Monte Carlo model, show in a very consistent way the existence and formation of vacancy-CrNiSiP clusters that play detrimental role in irradiation hardening. Similar solute cluster number density of about 30 to 50 $\times 10^{16} cm^{-3}$ and an average diameter of about 1 nm were estimated for all alloys containing minor solutes, irrespectively of the chromium content. In Fe9Cr ferritic and Fe9Cr ferritic/martensitic alloys, with significantly reduced concentration of minor solute elements, the main defects are vacancy clusters, with an average cluster size size of about 10 and 2 vacancies, respectively. Large concentration of α'-precipitates was observed in Fe14CrNiSiP. However, both vacancy clusters and α'-precipitates provide significantly less impact to hardening in comparison to vacancy-CrNiSiP clusters. The fact that vacancy clustering in Fe9Cr ferritic alloy resembles that of pure iron suggests that Cr solutes play minor role in irradiation hardening of ferritic/martensitic alloys and steels.

Keywords: Neutron irradiation, FeCr alloys and steels

1. Introduction

High Cr ferritic/martensitic (FM) steels are candidate structural materials for the construction of key components in future reactors, since they offer better

*Corresponding author
Email address: mkonstan@sckcen.be (M.J. Konstantinović)

radiation resistance in comparison to austenitic steels [1, 2, 3, 4]. GenIV and fusion reactors will operate at temperatures well above 400 °C, with neutron doses foreseen to be in the range of 50 to 100 dpa [5, 6]. FM steels are expected to be well suited to withstand these conditions, as they experience negligible swelling under neutron irradiation, offer good thermal conductivity and exhibit reduced thermal expansion.However, their potential use could be limited due to low temperature radiation embrittlement, which they experience when irradiated bellow 400 °C, even if the neutron dose is very low [7]. In search of minimal ductile-brittle transition temperature (DBTT) shift, the low temperature embrittlement behavior of F/M steels has been extensively studied as a function of the Cr content [8]. Accumulated results led to the empirical identification of the most optimal one to be at 9%Cr for reduced-activation F/M steels (T91, Eurofer97, F82H, HT9). Still, there is not yet full understanding of the role of the different alloying elements and initial microstructure on the degradation of mechanical properties of these steels under irradiation. From the modeling perspective, the minimum shift of DBTT at 9%Cr was largely ascribed to complex effects related with how Cr influences the microstructure evolution and redistributes itself under irradiation [9, 10]. Experimentally, in most cases it was difficult to separate and control different factors in order to deduce their individual contributions [14, 15].

Recently, the mechanical properties of neutron irradiated Fe-Cr ferritic model alloys, with minimal and similar C content, but with varying concentrations of Cr, Ni, Si and P, were investigated together with actual 9%Cr Cr F/M alloys [13]. The focus was on the effect on radiation hardening of the content of Cr and minor solutes such as Ni, Si and P, as well as on initial microstructure. Irrespective of irradiation temperature and of the Cr content, significant hardening was observed only in model alloys containing Ni, Si and P solute atoms, suggesting that Cr solutes play lesser role in irradiation hardening of ferritic/martensitic alloys steels than previously believed. The presence of minor solutes (Ni, Si, P) was found to be essential for the microstructural features that form under irradiation to have a hardening effect, i.e. to make the features efficient obstacles to dislocation motion. These results were found to be in a very good agreement with previous atom probe tomography (APT) studies that have revealed that solute clusters containing not only Cr, but also minor solutes, form under neutron irradiation at 300 °C [11, 12]. Additionally, it was observed that the martensitic alloys harden much less than the ferritic ones. It is possible that the limited hardening is partly a consequence of higher dislocation density, specific grain structure or carbon distribution in comparison to ferrites, which would influence distribution of vacancies and self intersititals leading to the reduced formation of solute clusters.

Therefore, in order to provide a solid interpretation of the mechanical property results that were reported in [13], a thorough microstructure examination is needed. In this study, the same neutron irradiated alloys that were previously mechanically tested are further investigated by positron annihilation spectroscopy (PAS) and small angle neutron scattering (SANS). The defect characterization based on these two techniques show without any doubt that

Table 1: The nominal composition of FeCr model alloys.

element (wt.%)	C	N	Si	P	S	Cr	Ni	Al	Fe
Fe9Cr FM	0.02	0.015	0.09	< 0.005	0.001	8.4	0.07	0.007	bal.
Fe9Cr	< 0.006	< 0.005	0.004	0.003	< 0.005	9.1	0.009	0.027	bal.
Fe9CrNiSiP	< 0.006	< 0.005	0.221	0.032	< 0.005	9.1	0.092	0.028	bal.
Fe5CrNiSiP	< 0.006	< 0.005	0.219	0.033	< 0.005	4.9	0.13	0.026	bal.
Fe14CrNiSiP	< 0.006	< 0.005	0.194	0.031	< 0.005	14.4	0.087	0.025	bal.

CrNiSiP clusters play the main role in irradiation hardening.

2. Materials, experiments and computation methods

2.1. Materials

Four ferritic and one FM model alloys has been investigated in this study. Their chemical composition is given in Table 1. Neutron irradiation was performed in the BR2 materials testing reactor of SCKCEN. Details on material fabrication and neutron irradiation were published elsewhere [13]. Microstructural investigation in this study have been performed on the samples that were irradiated at about 300 ^{0}C to neutron dose of 0.11 dpa.

2.2. PAS

Positron annihilation spectroscopy (PAS) experiments were performed with the Coincidence Doppler broadening spectrometer (CDB). The CDB spectra were measured using two Ge detectors. Details of the setup are described in [16]. CDB spectroscopy allows the measurement of the momentum distribution of the electron-positron pair and they are typically analyzed based on the S-parameter (line-shape parameter) and the W-parameter (wing parameter). The S and W-parameters are defined as the ratio of low momentum ($\mid p_L \mid < 2.5 \times 10^{-3} m_0 c$) and high momentum ($15 \times 10^{-3} m_0 c < \mid (p_L) \mid < 25 \times 10^{-3} m_0 c$) regions of the CDB spectra to the total momentum, respectively (where c is speed of light and p_L is the longitudinal component of the positron-electron momentum along the direction of γ-ray emission). The annihilation of positrons with valence electrons contributes to the low momentum region (S-parameter), thus providing information about open volume defects. On the other hand, the annihilation of positrons with inner shell electrons contributes to the high-momentum region (W-parameter)and provides information about chemical environment at annihilation site.

2.3. SANS and Vickers hardness

The small angle neutron scattering (SANS) measurements were carried out at the instrument PAXY at LLB Saclay (France) [17]. Samples of 1 mm thickness were placed in a magnetic field of 1.5 T oriented perpendicular to the incident neutron beam of 0.5 nm wavelength. Two sample-detector distances of

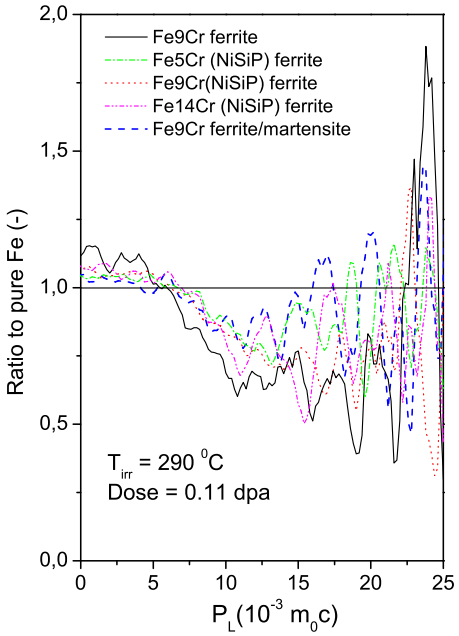

Figure 1: (Color online) Doppler broadening spectra of the FeCr alloys. Measurement error increases with P_L; minimum and maximum values are shown.

2 and 6 m with corresponding collimation lengths were chosen, thus covering a range of scattering vector, Q, from 0.05 to 2.5 nm^{-1}. The raw data treatment including transmission measurement and correction for both background and detector sensitivity is described in [18]. For absolute calibration a standard sample with known scattering cross section was used. Data analysis including separation of magnetic and nuclear scattering cross-sections was performed using the BerSANS software package [19]. The scattering cross-sections of the unirradiated reference samples were subtracted from the respective cross-sections of the irradiated samples in order to derive the characteristics of irradiation-induced scatterers. These difference scattering curves were transformed into size distributions of scatterers using an own code [20] based on the Monte Carlo method introduced by [21]. The volume fraction and number densities of scatterers in absolute units were obtained assuming non-magnetic scatterers (magnetic holes) in an Fe-9Cr matrix [22]. The A-ratio, A = 1 + M/N, was calculated from the magnetic (M) and nuclear (N) contributions of the scatterer. It is a one-parameter signature of the mean composition of irradiation-induced scatterers. A more detailed description about the A-ratio as function of the cluster composition is given in [23, 24].

Vickers hardness HV10 (load 98.1 N) was measured according to the standard DIN EN ISO 6507 using the unirradiated or irradiated SANS samples after the SANS experiments.

2.4. OKMC simulation

The Object Kinetic Monte Carlo (OKMC) model used in this study describes the evolution of an alloy under irradiation with stochastic events implementing the migration and interaction of diffusing species; these are point defects or complexes involving point defects and solutes, e.g., vacancy-solute clusters [25]. Key reactions in our OKMC model are the dragging of solute atoms by single point-defects, and the binding of solute atoms with small loops, which were parameterized based on DFT calculations [26]. The OKMC model within a "grey alloy" approximation, in which the effect of the alloying elements was translated into a change of the value of the parameters that define the mobility and stability of point defects and their clusters as a function of the nominal composition, has been previously successfully applied to reactor pressure vessel alloys [27, 28] and steels [29]. In order to be applied to concentrated Fe-Cr alloys, the "grey alloy" approximation in the OKMC model was kept only for the chromium atoms, while all other minor alloying elements are included explicitly. Thus, the OKMC model has been designed to describe the formation of vacancy clusters and NiSiP-rich clusters under irradiation, but cannot directly predict their Cr content, or the formation of α'-particles. This approximation is a compromise between the current capabilities of the OKMC technique and an explicit description of the formation of solute/point-defect clusters, which allows the results to be used for an assessment of the microstructural features that are expected to mainly cause radiation hardening.

3. Results and discussion

The CDB spectra of neutron-irradiated Fe-Cr alloys are shown in Fig.1. All irradiated materials exhibit an increase of the S-parameter and a decrease of the W-parameter, indicating that positrons are trapped and annihilate at vacancy-rich complexes induced by neutron irradiation. Clearly, Fe9Cr ferrite has the strongest enhancement in the low momentum region of all materials. In the high momentum region, the smallest difference with respect to the reference Fe sample (represented by the dashed straight line) was observed for Fe9Cr FM alloy. The CDB spectra of all other alloys fall in between these two extreme cases. The properties of vacancy rich clusters in these alloys are further studied based on the W vs S parametric plot. The plot showing the W-parameter versus the S-parameter of both non-irradiated and neutron irradiated Fe-Cr alloys is presented in Fig.2, including the data for irradiated pure Fe [30]. This graph illustrates the evolution of vacancy-rich clusters after irradiation in various alloys. Non-irradiated alloys, Fig.2a, exhibit slightly higher the S-parameter and lower the W-parameter than pure Fe, mainly due to higher dislocation density in these alloys with respect of pure Fe.

The results of CDB measurements for materials which are neutron irradiated at 290 °C, in the form of the W-parameter versus the S-parameter, are given in Fig.2 b. After neutron irradiation, a significant increase of the S-parameter, as compared to non-irradiated materials, is observed for all alloys except Fe9Cr

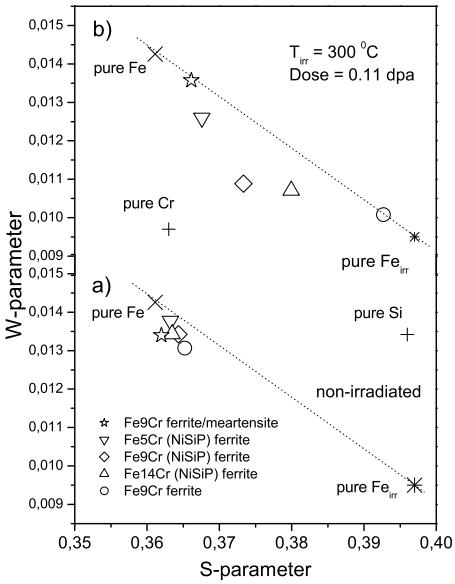

Figure 2: S versus W parameters of neutron irradiated FeCr alloys

FM. The largest increase of the S-parameter after neutron irradiation has been found for Fe9Cr. Overall, this is consistent with the known fact that ferrite develops more easily a void population than martensite [31]. This could indicate that the presence of Ni, Si and P solutes suppresses the growth of vacancy clusters, while Cr does not. Interestingly, the decrease of the W-parameter seems to be more than just the compensation to the increase of the S-parameter (narrowing of the CDB curve). In contrast to Fe9Cr and Fe9Cr FM, the S- and W-parameters of Fe5,9,14Cr(NiSiP) do not lay on the straight line connecting pure Fe and neutron irradiated Fe points. W-S points in these three materials are displaced towards lower values of the W-parameter in comparison to W-S evolution of irradiated pure Fe. Since the W-parameter provides information about chemical environment around annihilation site [32], these results indicate the formation of solute clusters.

The SANS spectra of Fe-Cr alloys are presented in Figs. 3 and 4. The magnetic SANS cross sections are presented in Fig.3 for ferritic Fe9Cr and Fe9Cr (NiSiP) alloys and in Fig.4 for the Fe9Cr FM alloy (Fe5,14CrNiSiP alloys exhibit similar SANS spectra as Fe9CrNiSiP and are not shown to save space). Increased scattering intensities of the irradiated states are observed for the range Q $>$ 0.3 nm-1 for all materials. For the range Q $<$ 0.3 nm-1, the scattering curves for the unirradiated and corresponding irradiated states approach each other and reach higher levels for Fe9Cr FM than for all ferritic alloys. Obviously, this is due to differences in the microstructure between both types of alloys, which are unchanged during irradiation, for instance the existence of carbides.

The estimated values of the A-ratio, volume fraction, number density and

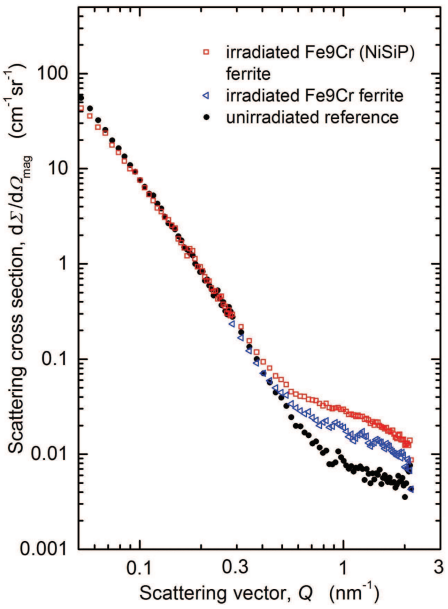

Figure 3: (Color online) Measured magnetic scattering cross-sections of pure Fe-9Cr, Fe9Cr (NiSiP) ferrite and unirradiated reference.

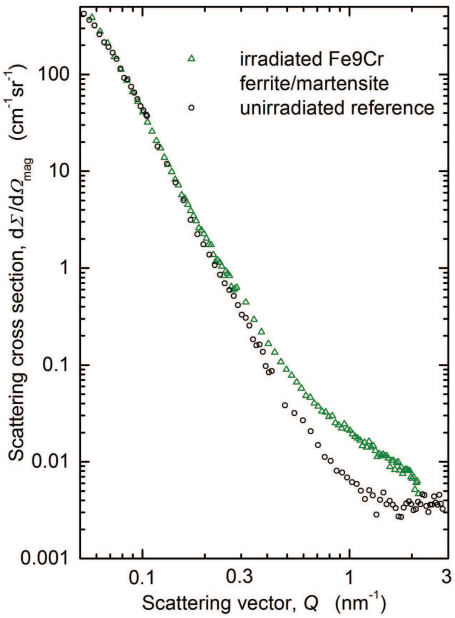

Figure 4: (Color online) Measured magnetic scattering cross sections of Fe9Cr ferrite/martensite and the unirradiated reference.

Table 2: Characteristics of irradiation-induced nano-features in Fe9Cr alloys irradiated up to 0.1 dpa derived by SANS (volume fraction c, number density N, mean radius R_{mean}, A-ratio), including the change of hardness value after irradiation Δ HV10)

material	c (vol %)	N ($\times 10^{16} cm^{-3}$)	R_{mean} (nm)	A-ratio	Δ HV10
Fe9CrC FM	0.13 ± 0.01	19±4	1.04 ± 0.07	2.20 ± 0.2	27±3
Fe9Cr ferrite	0.15 ± 0.01	39±8	0.90 ± 0.02	1.45± 0.1	22±3
Fe9Cr(NiSiP) ferrite	0.29 ± 0.01	69±12	0.95 ± 0.05	1.90± 0.15	72±3
Fe5Cr(NiSiP) ferrite	0.13 ± 0.01	27±3	0.97 ± 0.08	3.50 ± 0.5	68±4
Fe14Cr(NiSiP) ferrite	1.75 ± 0.05	592±76	0.83 ± 0.03	2.15 ± 0.15	94±7

mean size are listed in Table 2. The nuclear scattering curves were found to exhibit similar shapes as the magnetic scattering curves, see [24] for Fe9Cr FM. This indicates that nuclear and magnetic scatterers are the same objects - a prerequisite for the interpretation of the A-ratio in terms of composition. The A-ratio observed for ferritic pure Fe9Cr indicates that the majority of irradiation-induced scatterers are vacancy clusters. Indeed, vacancy clusters in Fe9Cr give rise to a theoretical A-ratio of 1.4 [24]. This observation is in an excellent agreement with the PAS data discussed above. The higher A-ratios of the other four alloys indicate a dominant contribution of solute clusters. It is worth to note that an A-ratio of 2.05 is expected for Cr-rich α'-phase particles [24], as observed in Fe14Cr(NiSiP). Moreover, the high volume fraction in Fe14Cr(NiSIP) provides additional argument for the presence of Cr-rich α'-phase particles in this alloy. However, if α'-particles were dominant in Fe9Cr(NiSiP) (A-ratio close to 2.05), they should also dominate in pure Fe9Cr, which is not the case. Therefore, it is reasonable to assume that the high A-ratio values in other three alloys are caused by other types of solute clusters, most probably CrNiSiP solute clusters [11]. The difference between A-ratios of Fe5Cr(NiSiP) and Fe9Cr(NiSIP) probably indicate different chemical composition of CrNiSiP solute clusters formed in these two alloys after neutron irradiation (e.g. different Cr content in the cluster) and/or different contribution from vacancy clusters. Note that the PAS data exhibit higher value of the S-parameter in Fe9Cr(NiSiP) as compared to Fe5Cr(NiSiP), which could already explain the lower value of the A-parameter in Fe9Cr(NiSiP) in comparison to Fe5Cr(NiSiP). The size distributions are similar for all ferritic alloys.

Hardness measurements were performed on the same set of samples as those used for PAS and SANS measurements. The results are summarized in Table 2. Significant hardness after neutron irradiation has been observed only in the alloys containing minor solute elements, namely Fe5.9.14Cr(NiSIP), which is in an excellent agreement with tensile tests [13]. Mechanical properties of these alloys suggest that Cr, even though present in large quantity in the alloy, as well as in the Cr-rich NiSiP clusters, is not the main cause of hardening. In fact, the presence of minor solutes (Ni, Si, P) is essential for the microstructural features that form under irradiation to have a hardening effect, i.e. to make the features efficient obstacles to dislocation motion.

Table 3: Characteristics of irradiation-induced vacancy and solute clusters in FeCr alloys irradiated up to 0.11 dpa derived by OKMC (number density N and average size). Average size of the vacancy cluster is presented as the number of vacancies in a cluster D_{vac}, while the average size of the solute cluster is shown as their average cluster diameter R_{sol}.

material	$N_{vac}(\times 10^{17} cm^{-3})$	$D_{vac}(\#)$	$N_{sol}(\times 10^{16} cm^{-3})$	R_{sol} (nm)
Fe9CrC FM	4.9	1.9	0	0
Fe9Cr ferrite	121	9.8	3.4	0.76
Fe9Cr(NiSiP) ferrite	34.0	2.0	48	0.93
Fe5Cr(NiSiP) ferrite	43.5	1.9	33	0.93
Fe14Cr(NiSiP) ferrite	37.1	2.1	34	0.94

With this in mind, we performed OKMC simulation to calculate the properties of vacancy and solute clusters formed under neutron irradiation, in which chromium atoms are taken into account in a "grey alloy" approximation, so that the formation of CrNiSiP solute clusters is governed mainly by the precipitation kinetics of Ni, Si and P. This assumption has been also supported by density functional theory [26], which predicts negligible binding energy of Cr to a vacancy. The OKMC results are summarized in Table 3. Even tough the OKMC calculation predicts the distribution of sizes of vacancy clusters to appear as a result of irradiation, the focus is given to the average values, since both PAS and SANS measurements provide only mean values. The formation of large vacancy clusters with an average size of about 10 vacancy per cluster has been obtained for Fe9Cr ferritic alloy. Clearly, this result is in full agreement with the PAS data, see Fig. 2, but it is mainly a consequence of the starting assumption that limits the role of chromium. Nevertheless, Cr reduces the mobility of self-interstitial clusters with respect to pure Fe, without affecting the vacancy mobility, leading to a vacancy population clusters slightly smaller than, but very similar to, the vacancy population in pure Fe. The size of vacancy cluster is drastically reduced to just a few vacancies per cluster in all other alloys. Evidently, the presence of Ni, Si and P solutes suppresses the growth of vacancy clusters in comparison to the Fe9Cr ferritic alloy, which leads to the decrease of the S-parameter in the PAS data. Small variations of the size of vacancy clusters in these alloys occurs due to the difference in minor solute concentrations, see Table 1. In contrast to ferritic alloys, the Fe9Cr FM alloy has been modeled with higher sink strength than in the case of ferritic alloys (two orders of magnitude higher dislocation density and lower grain size). In this case, the OKMC model predicts the number density of vacancy clusters close to the non-irradiated case (note that no solute cluster formation has been observed by OKMC in this alloy, see discussion below). However, vacancy clustering in Fe9Cr ferritic alloy irradiated to 0.11 dpa has limited effect on hardening, since the vacancy clusters are still to small to act as obstacles to dislocation motion. According to previous studies [15], significant effect of vacancy clustering on hardening in FeCr alloys is expected at about 0.5 dpa and more.

The OKMC model calculation also provides information about the solute clusters. An average cluster size with a diameter of about 1 nm has been ob-

served for all alloys, irrespectively of their chemical composition. These results are found to be in excellent agreement with the SANS results. Good quantitative agreement between the OKMC model with the SANS results has been also observed for what concerns the solute cluster number density, see Tables 2 and 3. In the case of neutron irradiation up to 0.11 dpa, a solute cluster number density of about 30 to 50 $\times 10^{16} cm^{-3}$ is expected in these alloys. The Fe9Cr ferritic alloy exhibits about 5 times lower solute cluster density than Fe9CrNiSiP, while no solute clusters were found in Fe9Cr FM. In the Fe9Cr ferritic alloy, the growth of solute clusters is minimal because of the low concentration of minor solutes, while in Fe9Cr FM no solute clusters are mainly the result of high sink strength. This effect is similar to the suppression of the growth of vacancy clusters. The solute number density calculated by the OKMC model in Fe5CrNiSiP alloy has been observed to be slightly lower than in the case of Fe9CrNiSiP and Fe14CrNiSiP. Most probably, this reduction occurs as a consequence of the variation in the mobility of self-interstitial cluster for different chromium concentrations, which is an integral part of the "grey" alloy approximation. This effect could potentially lead to the different solute cluster compositions that should show up in the values of the A-parameter. Indeed, the A-parameter of Fe5Cr(NiSIP) exhibits very different values in comparison to other alloys. However, the model is not detailed enough to allow an assessment of origin of the significantly higher A ratio that was measured in the case of the Fe5Cr(NiSIP) alloy. Finally, as expected, the OKMC model largely underestimate the solute cluster concentration in Fe14CrNiSiP alloy, since it cannot predict the formation of α' particles.

4. Conclusions

PAS, SANS and hardness experiments were performed on neutron irradiated FeCr alloys. Hardness measurements were found to be in excellent agreement with the tensile test results published previously. They confirm the existence of irradiation hardening only in alloys containing minor solute elements. Moreover, both PAS and SANS experiments confirm in a consistent way the formation of large vacancy clusters in the Fe9Cr ferrite. Since only minor solute clustering has been observed by both experiments in this alloy (due to some impurities), it can be concluded with confidence that the chromium atoms play limited role in irradiation hardening. In all ferritic alloys containing minor solutes, vacancy-CrNiSIP clusters are clearly observed by both PAS and SANS experiments. In PAS, the existence of vacanacy-CrNiSIP clusters is manifested by the significant difference of the W-parameter with respect to those expected in both pure Fe or Fe9Cr alloys without minor solute elements. In SANS, their existence has been confirmed by the measurements of the defect volume fraction (number density) and the A-parameter. Most experimental results can be rationalized based on the OKMC model, which is implemented in a "grey alloy" approximation only for the chromium atoms, while all other alloying elements were included explicitly. Significant number of α' particles were observed in Fe14(NiSIP).

However, both vacancy clusters and α'-precipitates impact hardening less in comparison to vacancy-CrNiSiP clusters.

Acknowledgements This work has received funding from the Euratom research and training programme 2014-2018 under grant agreement No. 755039 (M4F project). This work also contributes to the Joint Programme on Nuclear Materials (JPNM) of the European Energy Research Alliance (EERA).

5. Data availability

The raw/processed data required to reproduce these findings cannot be shared at this time as the data also forms part of an ongoing study.

References

[1] R.L. Klueh, D.R. Harris, High chromium ferritic martensitic steels for nuclear applications, ASTM (2001).

[2] R.L. Klueh, A.T. Nelson, J. Nucl. Mater, Ferritic steels for next-generation reactors, 371 (2007) 37-52.

[3] S. J. Zinkle, J. T. Busby, Structural materials for fission and fusion energy, Materials Today 12 (2009) 12.

[4] N. Singh, J.H. Evans, J. Nucl. Mater, Significant differences in defect accumulation behaviour between fcc and bcc crystals under cascade damage conditions, 226 (1995) 277-285.

[5] P. Yvon and F. Carré, Structural materials challenges for advanced reactor systems, J. Nucl. Mater 385 (2009) 217-222.

[6] A. Zinkle, H. Muroga, S.J. Möslang, T. Tanigawa, Multimodal options for materials research to advance the basis for fusion energy in the ITER era, Nucl. Fusion, 53 (2013) 104024.

[7] Y. Chen, Irradiation effects of HT-9 martensitic steel, Nucl. Eng. and Technol. 45 (2013) 311.

[8] A. Kohyama, A. Hishinuma, D.S. Gelles, R.L. Klueh, W. Dietz, K. Ehrlich, Low-activation ferritic and martensitic steels for fusion application, J. Nucl. Mater. 233-237 (1996) 138-147.

[9] L. Malerba, G. Bonny, D. Terentyev, E.E. Zhurkin, M. Hou, K. Vörtler, K. Nordlund, Microchemical effects in irradiated Fe-Cr alloys as revealed by atomistic simulation, Journal of Nuclear Materials 442 (2013) 486-498.

[10] D. Terentyev, G. Bonny, C. Domain, G. Monnet, L. Malerba, Mechanisms of radiation strengthening in FeCr alloys as revealed by atomistic studies, Journal of Nuclear Materials 442 (2013) 470-485.

[11] V. Kuksenko, C. Pareige, C. Genevois, F. Cuvilly, M. Roussel, P. Pareige, Effect of neutron-irradiation on the microstructure of a Fe12at.%Cr alloy, J. Nucl. Mater. 415 (2011) 61-66.

[12] B. Gómez-Ferrer, C. Heintze, C. Pareige, On the role of Ni, Si and P on the nanostructural evolution of FeCr alloys under irradiation, J. Nucl. Mater. 517 (2019) 35-44.

[13] M.J. Konstantinović, M. Lorenzo, Mechanical properties of FeCr alloys after neutron irradiation, J. Nucl. Mater. 528 (2020) 151879.

[14] M. Matijašević and A. Almazouzi, Effect of Cr on the mechanical properties and microstructure of FeCr model alloys after n-irradiation, J. Nucl. Mater. 377 (2008) 147-154.

[15] M.J. Konstantinović, W. Van Renterghem, M. Matijašević, B. Minov, M. Lambrecht, T. Toyama. M. Chiapetto and L. Malerba, Mechanical and microstructural properties of neutron irradiated FeCrC alloys, Phys. Status Solidi (A), 213 (2016) 2988-2994.

[16] K. Verheyen, M. Jardin, A. Almazouzi, Coincidence Doppler broadening spectroscopy in Fe, FeC and FeCu after neutron irradiation, J. Nucl. Mater. 351 (2006) 209-215.

[17] http://www-llb.cea.fr/fr-en/pdf/paxy-llb.pdf

[18] P. Strunz, J. Saroun, U. Keiderling, A. Wiedenmann, R. Przenioslo, General formula for determination of cross-section from measured SANS intensities, J. Appl. Cryst. 33 (2000) 829-833.

[19] U. Keiderling, The new 'BerSANS-PC' software for reduction and treatment of small angle neutron scattering data, Appl. Phys. A 74 (2002) S1455-1457.

[20] A. Wagner, F. Bergner, A. Ulbricht, C.D. Dewhurst, Small-angle neutron scattering of low-Cu RPV steels neutron-irradiated at 255 °C and post-irradiation annealed at 290 °C, J. Nucl. Mater 441 (2013) 487-492.

[21] S. Martelli, P.E. Di Nunzio, Particle Size Distribution of Nanospheres by Monte Carlo Fitting of Small Angle X-Ray Scattering Curves, Part. Part. Syst. Charact. 19 (2002) 247e255.

[22] S. Mühlbauer, D. Honecker, É. A. Périgo, F. Bergner, S. Disch, A. Heinemann, S. Erokhin, D. Berkov, C. Leighton, M. R. Eskildsen, A. Michels, Magnetic small-angle neutron scattering, Rev. Mod. Phys. 91 (2019) 015004 pp75.

[23] A. Ulbricht, F. Bergner, J. Böhmert, M. Valo, M.-H. Mathon, A. Heinemann, SANS response of VVER440-type weld material after irradiation, post-irradiation annealing and reirradiation, Phil. Mag. 87 (2007) 1855-1870.

[24] C. Heintze, F. Bergner, A. Ulbricht, H. Eckerlebe, The microstructure of neutron-irradiated Fe-Cr alloys: A small-angle scattering study, J. Nucl. Mater. 409 (2011) 106-111.

[25] N. Castin, G. Bonny, A. Bakaev, F. Bergner, C. Domain, J.M. Hyde, L. Messina, B. Radiguet and L. Malerba, The dominating mechanisms for the formation of solute-rich clusters in steels under irradiation, arXiv:1912.06828 [cond-mat.mtrl-sci].

[26] C. Domain, C. Domain, C.S. Becquart, Solute $< 111 >$ interstitial loop interaction in α-Fe: A DFT study, J. Nucl. Mater. 499 (2018) 582-594.

[27] M. Chiapetto, L. Malerba, C.S. Becquart, Nanostructure evolution under irradiation in FeMnNi alloys: A "grey alloy" object kinetic Monte Carlo model, J. Nucl. Mater. 462 (2015) 91-99.

[28] M. Chiapetto, C.S. Becquart, C. Domain, L. Malerba, Nanostructure evolution under irradiation of Fe(C)MnNi model alloys for reactor pressure vessel steels, Nucl. Instrum. Methods Phys. Res. B 352 (2015) 56-60.

[29] M.J. Konstantinović, I. Uytdenhouwen, G. Bonny, N. Castin, L. Malerba and P. Efsing, Radiation induced solute clustering in high-Ni reactor pressure vessel steel, Acta Mat. 179 (2019) 183-189.

[30] M. Lambrecht, L. Malerba, A. Almazouzi, Influence of different chemical elements on irradiation-induced hardening embrittlement of RPV steels, J. Nucl. Mater. 378 (2008) 282.

[31] V. Bryk, O. Borodin, A. Kalchenko, V. Voyevodin, V. Ageev, A. Nikitina, V. Novikov, V. Inozemtsev, A. Zeman, F. Garner, in: proceedings of the 11th International Topical Meeting on Nuclear Applications of Accelerators, AccApp 2013, Bruges, Belgium, (2013).

[32] Y. Nagai, M. Hasegawa, Z. Tang, A. Hempel, Y. Kawazoe, A. Kawai, F. Kano, Positron confinement in ultrafine embedded particles: Quantum-dot-like state in an Fe-Cu alloy, Phys. Rev. B 61 (2000) 6574-6578.